An astronomically dated record of Earth's climate and its predictability over the last 66 Million Years

Authors: Thomas Westerhold[1*], Norbert Marwan[2,3], Anna Joy Drury[1,4], Diederik Liebrand[1], Claudia Agnini[5], Eleni Anagnostou[6], James S. K. Barnet[7,8], Steven M. Bohaty[9], David De Vleeschouwer[1], Fabio Florindo[10,11], Thomas Frederichs[1,12], David A. Hodell[13], Ann E. Holbourn[14], Dick Kroon[15], Vittoria Lauretano[16], Kate Littler[7], Lucas J. Lourens[17], Mitchell Lyle[18], Heiko Pälike[1], Ursula Röhl[1], Jun Tian[19], Roy H. Wilkens[20], Paul A. Wilson[9], James C. Zachos[21]

Affiliations:

[1]MARUM – Center for Marine Environmental Sciences, University of Bremen, 28359 Bremen, Germany.

[2]Member of the Leibniz Association, Potsdam Institute for Climate Impact Research (PIK), 14412 Potsdam, Germany

[3]University of Potsdam, Institute of Geosciences, 14469 Potsdam, Germany

[4]Department of Earth Sciences, University College London, Gower Street, London, WC1E 6BT, UK.

[5]Dipartimento di Geoscienze, Università degli Studi di Padova, Via Gradenigo 6, I-35131 Padova, Italy.

[6]GEOMAR Helmholtz-Zentrum für Ozeanforschung Kiel, Wischhofstrasse 1-3, 24148 Kiel, Germany.

[7]Camborne School of Mines and Environment and Sustainability Institute, University of Exeter, Penryn Campus, Penryn, UK.

[8]School of Earth and Environmental Sciences, University of St Andrews, St Andrews, Scotland, UK

[9]Ocean and Earth Science, University of Southampton, National Oceanography Centre, Southampton, UK.

[10]Istituto Nazionale di Geofisica & Vulcanologia, INGV, Rome, Italy.

[11]Institute for Climate Change Solutions, Pesaro e Urbino, Italy

[12]Faculty of Geosciences, University of Bremen, Bremen, Germany.

[13]Godwin Laboratory for Palaeoclimate Research, Department of Earth Sciences, University of Cambridge, Cambridge, UK.

[14]Institute of Geosciences, Christian-Albrechts-University, Kiel 24118, Germany.

[15]School of GeoSciences, University of Edinburgh, Edinburgh, UK.

[16]School of Chemistry, University of Bristol, Bristol BS8 1TS, UK.

[17]Department of Earth Sciences, Faculty of Geosciences, Utrecht University, Princetonlaan 8a, 3584 CB Utrecht, Netherlands.

[18]College of Earth, Ocean, and Atmospheric Science, Oregon State University, Corvallis, Oregon 97331, USA.

[19]State Key Laboratory of Marine Geology, Tongji University, Siping Road 1239, Shanghai 200092, PR China.

[20]University of Hawaii, School of Ocean and Earth Science and Technology, Honolulu Hawaii 96822, USA.

[21]Department of Earth and Planetary Sciences, University of California Santa Cruz, California, USA.

*Correspondence to: twesterhold@marum.de

Abstract:

Much of our understanding of Earth's past climate comes from the measurement of oxygen and carbon isotope variations in deep-sea benthic foraminifera. Yet, long intervals in existing records lack the temporal resolution and age control needed to thoroughly categorize climate states of the Cenozoic Era and to study their dynamics. Here we present a new, highly resolved, astronomically dated, continuous composite of benthic foraminifer isotope records developed in our laboratories. Four climate states – Hothouse, Warmhouse, Coolhouse, Icehouse – are identified based on their distinctive response to astronomical forcing depending on greenhouse gas levels and polar ice sheet volume. Statistical analysis of the non-linear behavior encoded in our record reveals the key role that polar ice volume plays in the predictability of Cenozoic climate dynamics.

One Sentence Summary:

During the last 66 million years Earth's climate system response to astronomical forcing was state-dependent.

Global changes in Earth's climate during the Cenozoic Era, the last 66 million years, have long been inferred from stable isotope data in carbonate shells of benthic foraminifers, which are single-celled amoeboid organisms that live on the seafloor. Carbon and oxygen isotope records from deep-sea benthic foraminifers are a proven, invaluable archive of long-term changes in Earth's carbon cycle, deep-sea temperature, and seawater composition driven by changes in ice volume (*1, 2*). In 1975, Shackleton and Kennett (*3*) produced one of the first deep-sea benthic foraminifer stable isotope records of the Cenozoic. Despite being of low temporal resolution it revealed that Earth's climate had transitioned from a warm state 60 to 40 million years ago (Ma) to a cool state 10 to 5 Ma. Over the last 45 years, many deep-sea benthic foraminifer stable isotope records of variable length and quality have been developed, resulting in a more detailed record of Cenozoic climate change. Compilations of these deep-sea isotope records provide a compelling chronicle of past trends, cyclic variations, and transient events in the climate system from the Late Cretaceous to today (*1, 4-10*). However, even the most recent benthic isotope compilations cannot accurately document the full range and detailed characteristics of Cenozoic climate variability on time scales of ten thousand to one million years. Age models and temporal resolution of Cenozoic benthic isotope compilations are either too coarse and/or include gaps, particularly prior to 34 Ma. These weaknesses hamper progress in determining the dynamics of the Cenozoic climate system (*4, 9, 11*), for example, because they prohibit application of advanced techniques of non-linear time series analysis at the required (astronomical) time-scales. The lack of highly-resolved, continuous, and accurately dated records constitutes a key limitation in our ability to identify and understand the characteristics of Earth's evolving climate during the Cenozoic.

Here, we present a new astronomically tuned deep-sea benthic foraminifer carbon $\delta^{13}C$ and oxygen $\delta^{18}O$ isotope reference record uniformly covering the entire Cenozoic, developed in our laboratories using sediment archives retrieved by scientific ocean drilling (Fig. 1). To produce this new composite record, we selected 14 ocean drilling records, checked and revised their composite splices where necessary, and preferentially selected records utilizing the genus *Cibicidoides* and *Nuttallides* to minimize systematic interspecies isotopic offsets (*1, 4, 12, 13*). We additionally generated new benthic stable isotope data spanning the late Miocene and middle-to-late Eocene to fill intervals inadequately covered by existing records. We collated existing astrochronologies for all records, recalibrated them to the La2010b orbital solution (*14*) if required, and developed a new astrochronology for the middle-to-late Eocene (*13*). We estimate our chronology to be accurate to ± 100-kyr for the Paleocene and Eocene, ± 50-kyr for the Oligocene to middle Miocene, and ± 10-kyr for the late Miocene to Pleistocene. The composite record is affected by some spatial bias arising from the uneven distribution of deep-sea stable isotope data that mainly derive from low- to mid-latitudes (*13*). Nevertheless, the resulting new **Ceno**zoic **G**lobal **R**eference benthic foraminifer carbon and oxygen **I**sotope **D**ataset (CENOGRID) provides a refined record with higher signal-to-noise ratio than any previous compilations ((*13*); text S1), and better coverage of the Paleocene, Eocene and late Miocene intervals (Fig. S32). The CENOGRID serves as an astronomically tuned high-definition stratigraphic reference of past global climate evolution for the past 66 million years.

On time scales of ten thousand to one million years, global climate is a complex, dynamical system responding non-linearly to quasi-periodic astronomical forcing. By combining the latest high-resolution generation of Cenozoic deep-sea isotope records on a highly accurate timescale, CENOGRID enables the definition of Earth's fundamental climates and investigation of the

predictability of their dynamics. We used recurrence analysis (RA) of the CENOGRID record (*13, 15*) to identify fundamental climate states that internally share characteristic and statistically distinctive dynamics. Recurrence is a major property of dynamical systems and RA provides information about non-linear dynamics, dynamical transitions, and even non-linear interrelationships (*15*), and facilitates evaluation of underlying dynamical processes – e.g., whether they are stochastic, regular, or chaotic. We present recurrence plots and their quantification of the benthic foraminifer $\delta^{13}C$ and $\delta^{18}O$ records to recognize different climate states and apply the RA measure of 'determinism' (DET) to quantify the predictability of Cenozoic climate dynamics.

Four distinctive climate states emerge as distinct blocks from our recurrence plots of the $\delta^{18}O$ CENOGRID record that we label Hothouse, Warmhouse, Coolhouse, and Icehouse state (Fig. 2). Block-like structures in the recurrence plots identify epochs where the dynamical system is 'trapped' in a particular state. This interpretation of Cenozoic climate history is broadly consistent with previous interpretations but our recurrence plot analysis of the highly resolved CENOGRID data provides a more statistically robust and objective exposition of events.

Detailed features of the four climate states can be inferred from the isotope profiles (Fig. 1) and scatter plots of the CENOGRID $\delta^{13}C$ and $\delta^{18}O$ data, and atmospheric CO_2 concentration estimates (Fig. 2; (*13)*). Warmhouse and Hothouse states prevailed from the Cretaceous/Paleogene boundary (K/Pg, 66 Ma) to the Eocene-Oligocene Transition (EOT, 34 Ma). During the Warmhouse, global temperatures were more than 5°C warmer than today (*13*) and benthic $\delta^{13}C$ and $\delta^{18}O$ show a persistent positive correlation with one another. The Hothouse operated between the Paleocene-Eocene Thermal Maximum at 56 Ma and the end of the Early Eocene Climate Optimum (EECO) at 47 Ma (*16*), when temperatures were more than 10°C

warmer than today and displayed greater amplitude variability. Transient warming events (hyperthermals) are an intrinsic feature of the Hothouse, wherein paired negative excursions in $\delta^{13}C$ and $\delta^{18}O$ reflect warming globally through rapid addition of carbon to the ocean-atmosphere system. The two Warmhouse phases from 66 to 56 Ma (Paleocene) and 47 to 34 Ma (middle-late Eocene) share a similar temperature range but have distinct background $\delta^{13}C$ isotope values and atmospheric CO_2 levels (Fig. 2, S35). At the EOT, the Warmhouse transitioned into the Coolhouse state, marked by a stepwise, significant drop in temperature and a major increase in continental ice volume with large ice-sheets appearing on Antarctica (*17*) to establish a unipolar glacial state (*18*). The recurrence plots mark out the EOT as the most prominent transition of the whole Cenozoic, which highlights the important role of ice sheets in modulating Earth's climate state (Fig. S33; (*13)*).

The Coolhouse state spans ~34 Ma (EOT) to 3.3 Ma (mid Pliocene M2 glacial), and is divided into two phases by the marked shift in $\delta^{18}O$ increase at 13.9 Ma related to the expansion of Antarctic ice sheets during the middle Miocene Climate Transition (mMCT; (*19)*). Warmer conditions culminating in the Miocene Climatic Optimum (MCO; ~17-14 Ma; (*20*)) characterize the first phase, followed by cooling and increasing $\delta^{18}O$ during the second phase (Fig 2). RA of carbon isotope data documents an additional major transition in the carbon cycle around 7 Ma related to end of the late Miocene Carbon Isotope Shift (*11, 21, 22*). A major change in the correlation between benthic foraminifer $\delta^{13}C$ and $\delta^{18}O$ occurs during the Pliocene epoch (*23*). The Icehouse climate state (Fig. 2), driven by the appearance of waxing and waning ice sheets in the northern hemisphere, was fully established by the Pliocene-Pleistocene transition (*24*) (Fig. 1, 2) with Marine Isotope Stage M2 at 3.3 Ma being a possible harbinger. The recurrence plots are less pronounced and more transparent from 3.3 Ma to today (Fig. 2, S34), suggesting that

Earth's climate-cryosphere dynamics entered a state not comparable to anything seen in the preceding 60 or more million years.

The CENOGRID allows us to scrutinize the state-dependency of climate system response to CO_2 and astronomical forcing on ten thousand to one million year time scales (*13*). Astronomical forcing throughout the Cenozoic is consistently uniform, but the RA indicates that the non-linear response in climate variability to this forcing is strongly influenced by the fundamental state of climate. Evolutionary spectrograms characterize the dominant climatic response to astronomical forcing during the Cenozoic (Fig. 3). We find that the prevailing climate state as characterized by atmospheric CO_2 concentration and polar ice sheets seems to orchestrate the response and impact of climate processes to astronomical forcing. Modeled insolation-driven global temperature variability on astronomical time scales suggest that different temperature response regimes exist: eccentricity dominates temperature responses in low latitudes, precession in mid latitudes and obliquity in high latitudes (*25*). Thus, pronounced astronomical cyclicity in the CENOGRID could reflect climate-state dependent amplifications of latitude-specific climate processes.

In the Hothouse and Warmhouse, as well as the first Coolhouse phase, eccentricity-related cycles dominate the CENOGRID indicating a strong influence of low-latitude processes on climate variations. Obliquity-related cycles are sparse in these intervals, but have been documented in other geochemical records (*26, 27*) exhibiting perhaps local lithological responses. Weak response in the obliquity-band during the Hothouse and Warmhouse intervals might be related to the absence of a high-latitude ice sheet that could have amplified climate response to obliquity forcing. The driving mechanism for the prevailing eccentricity cyclicity in the benthic $\delta^{13}C$ and $\delta^{18}O$ records is still unknown, but modeling suggests that low- and mid-latitude processes in the climate system respond in a non-linear way to insolation forcing (*25*, *28-30*). In this regard, a key

feedback likely involves the hydrological cycle with highly seasonal precipitation patterns during intervals of strong monsoon response to precession-induced insolation change which could play a major role in the global distribution of moisture and energy (*31-34*). The expression of precession is apparently weak in the CENOGRID composite record despite the dominant eccentricity forcing, likely due to the long residence time of carbon in the oceans enhancing longer forcing periods (*30, 35*), as well as our strategy to avoid 'overtuning' the record. Following the increasing influence of high latitude cooling and ice growth during the second Coolhouse phase, the obliquity-band response steadily increases after the mMCT before dominating climate dynamics by the late Miocene-early Pliocene (*11, 22, 36*). In the Icehouse state, the progressive decrease in atmospheric CO_2 and major growth of polar ice sheets, which enhanced variability in $\delta^{18}O$, steadily amplified the influence of complex high latitude feedbacks until they essentially dominate climate dynamics.

To better understand the complexity of climate dynamics recorded in the CENOGRID, we computed the RA measure of determinism (DET, (*13)*). This parameter quantifies the predictability of dynamics in a system's state. Predictability estimates the stochastic (unpredictable) versus the deterministic (predictable) nature of climate dynamics recorded in CENOGRID (*13*). DET values near zero correspond to unpredictable dynamics, whereas large values indicate predictable dynamics, which are especially interesting to examine on the approach to tipping points. Changes in DET can thus reveal transitions between fundamentally different climate regimes.

Our RA suggests that climate dynamics during the Warmhouse and Hothouse Cenozoic states are more predictable or more regular than those of the Coolhouse and Icehouse states (Fig. 3). The growth of polar ice sheets at the EOT enhanced the effect of obliquity pacing of high

latitude climate that interacted with eccentricity-modulated precession forcing at lower latitudes from that point in time. This led to increased non-linear interactions among astronomically paced climate processes, and thus more complex, stochastic climate dynamics. The development of large Antarctic ice volume at the inception of the Coolhouse is associated with a fundamental regime change towards less predictable climate variability (lower DET values calculated from benthic $\delta^{18}O$, Fig. 3). From 25 to 13.9 Ma DET is elevated again, related to a reduction in ice volume in relatively warmer times of the Coolhouse, culminating in the MCO. Despite the growing influence of ice sheets in the Coolhouse, until ~6 to 7 Ma carbon cycle dynamics remain more deterministic than temperature because $\delta^{13}C$ variations are predominantly driven by low-latitude processes and less strongly influenced by the complex interaction with polar ice-sheet fluctuations. After ~6 Ma DET drops likely due to stronger cryosphere imprint on the carbon cycle. Upon initiation of the Icehouse at 3.3 Ma, $\delta^{18}O$ recorded climate dynamics become slightly more deterministic (*37*) and carbon cycle dynamics unpredictable, likely resulting from the complex response to the waxing and waning of polar caps (*38*).

The CENOGRID spectrogram displays a broader frequency range during several intervals with low DET values (e.g., Coolhouse), while high DET values (e.g., Warmhouse) occur when single frequencies dominate (Fig. 3). This could be signaling a more direct response to astronomical forcing in the Warmhouse compared to the Coolhouse. Our RA suggests that the Hothouse is more stochastic (less predictable) than the Warmhouse, presumably induced by the occurrence of extreme hyperthermal events and their strong non-linear and much amplified climate response to astronomical forcing (*39, 40*). The evolving pattern in the DET from the onset of cooling after the EECO to the EOT is striking (Fig. 3). The amplitude in fluctuations between stochastic and deterministic dynamics intensifies from 49 Ma to 34 Ma, consistent with how Earth's climate

system is suggested to behave (*41, 42*) as it moves towards a major tipping point. Once that tipping point is reached at the EOT, a rapid shift toward more permanently stochastic dynamics marks the inception of a new climate state (*43*). Thus polar ice volume is not only critical to defining Earth's fundamental climate state, it also seems to play a critical role in determining the predictability of its climatological response to astronomical forcing.

References and Notes:

1. J. Zachos, M. Pagani, L. Sloan, E. Thomas, K. Billups, Trends, Rhythms, and Aberrations in Global Climate 65 Ma to Present. *Science* **292**, 686-693 (2001).
2. K. G. Miller, G. Mountain, J. D. Wright, J. V. Browning, A 180-Million-Year Record of Sea Level and Ice Volume Variations from Continental Margin and Deep-Sea Isotopic Records. *Oceanography* **24**, 40-53 (2011).
3. N. J. Shackleton, J. P. Kennett, in *Init. Repts. DSDP , 29: Washington (U.S. Govt. Printing Office),* J. P. Kennett, R. E. Houtz, et al., Eds. (1975), pp. 743-755.
4. B. S. Cramer, J. R. Toggweiler, J. D. Wright, M. E. Katz, K. G. Miller, Ocean overturning since the Late Cretaceous: Inferences from a new benthic foraminiferal isotope compilation. *Paleoceanography* **24**, (2009).
5. D. De Vleeschouwer, M. Vahlenkamp, M. Crucifix, H. Pälike, Alternating Southern and Northern Hemisphere climate response to astronomical forcing during the past 35 m.y. *Geology* **45**, 375-378 (2017).
6. O. Friedrich, R. D. Norris, J. Erbacher, Evolution of middle to Late Cretaceous oceans – A 55 m.y. record of Earth's temperature and carbon cycle. *Geology* **40**, 107-110 (2012).
7. K. G. Miller, R. G. Fairbanks, G. S. Mountain, Tertiary oxygen isotope synthesis, sea level history, and continental margin erosion. *Paleoceanography* **2**, 1-19 (1987).
8. J. Veizer, A. Prokoph, Temperatures and oxygen isotopic composition of Phanerozoic oceans. *Earth-Science Reviews* **146**, 92-104 (2015).
9. J. C. Zachos, G. R. Dickens, R. E. Zeebe, An early Cenozoic perspective on greenhouse warming and carbon-cycle dynamics. *Nature* **451**, 279-283 (2008).
10. K. G. Miller et al., Cenozoic sea-level and cryospheric evolution from deep-sea geochemical and continental margin records. *Science Advances* **6,** no. 20, (2020).
11. A. J. Drury, T. Westerhold, D. Hodell, U. Röhl, Reinforcing the North Atlantic backbone: revision and extension of the composite splice at ODP Site 982. *Clim. Past* **14**, 321-338 (2018).
12. M. E. Katz *et al.*, Early Cenozoic benthic foraminiferal isotopes: Species reliability and interspecies correction factors. *Paleoceanography* **18**, 10.1029/2002PA000798 (2003).
13. See supplementary materials.
14. J. Laskar, A. Fienga, M. Gastineau, H. Manche, La2010: a new orbital solution for the long-term motion of the Earth. *Astronomy and Astrophysics* **532**, 15 (2011).
15. N. Marwan, M. C. Romano, M. Thiel, J. Kurths, Recurrence plots for the analysis of complex systems. *Physics Reports* **438**, 237-329 (2007).
16. T. Westerhold, U. Röhl, B. Donner, J. C. Zachos, Global Extent of Early Eocene Hyperthermal Events: A New Pacific Benthic Foraminiferal Isotope Record From Shatsky Rise (ODP Site 1209). *Paleoceanography and Paleoclimatology* **33**, 626-642 (2018).
17. H. K. Coxall, P. A. Wilson, H. Pälike, C. H. Lear, J. Backman, Rapid stepwise onset of Antarctic glaciation and deeper calcite compensation in the Pacific Ocean. *Nature* **433**, 53-57 (2005).
18. J. F. Spray *et al.*, North Atlantic Evidence for a Unipolar Icehouse Climate State at the Eocene-Oligocene Transition. *Paleoceanography and Paleoclimatology* **34**, 1124-1138 (2019).

19. B. P. Flower, J. P. Kennett, The middle Miocene climatic transition: East Antarctic ice sheet development, deep ocean circulation and global carbon cycling. *Pal. Pal. Pal.*, **108**, 537-555 (1994).
20. A. E. Holbourn, W. Kuhnt, K. G. D. Kochhann, N. Andersen, K. J. S. Meier, Global perturbation of the carbon cycle at the onset of the Miocene Climatic Optimum. *Geology* **43**, 123-126 (2015).
21. D. A. Hodell, K. A. Venz-Curtis, Late Neogene history of deepwater ventilation in the Southern Ocean. *Geochemistry, Geophysics, Geosystems* **7**, (2006).
22. A. J. Drury *et al.*, Late Miocene climate and time scale reconciliation: Accurate orbital calibration from a deep-sea perspective. *Earth and Planetary Science Letters* **475**, 254-266 (2017).
23. S. Kirtland Turner, Pliocene switch in orbital-scale carbon cycle/climate dynamics. *Paleoceanography* **29**, 1256-1266 (2014).
24. I. Bailey *et al.*, An alternative suggestion for the Pliocene onset of major northern hemisphere glaciation based on the geochemical provenance of North Atlantic Ocean ice-rafted debris. *Quaternary Science Reviews* **75**, 181-194 (2013).
25. T. Laepple, G. Lohmann, Seasonal cycle as template for climate variability on astronomical timescales. *Paleoceanography* **24**, (2009).
26. T. Westerhold, U. Röhl, High resolution cyclostratigraphy of the early Eocene - new insights into the origin of the Cenozoic cooling trend. *Climate of the Past* **5**, 309-327 (2009).
27. M. Vahlenkamp et al., Astronomically paced changes in deep-water circulation in the western North Atlantic during the middle Eocene. *Earth and Planetary Science Letters* **484**, 329-340 (2018).
28. T. J. Crowley, K.-Y. Kim, J. G. Mengel, D. A. Short, Modeling 100,000 year climate fluctuations in pre-Pleistocene time series. *Science* **255**, 705-707 (1992).
29. D. A. Short, J. G. Mengel, T. J. Crowley, W. T. Hyde, G. R. North, Filtering of Milankovitch Cycles by Earth's Geography. *Quaternary Research* **35**, 157-173 (1991).
30. R. E. Zeebe, T. Westerhold, K. Littler, J. C. Zachos, Orbital forcing of the Paleocene and Eocene carbon cycle. *Paleoceanography* **32**, 440-465 (2017).
31. K. E. Trenberth, D. P. Stepaniak, J. M. Caron, The Global Monsoon as Seen through the Divergent Atmospheric Circulation. *Journal of Climate* **13**, 3969-3993 (2000).
32. P. X. Wang *et al.*, The global monsoon across time scales: Mechanisms and outstanding issues. *Earth-Science Reviews* **174**, 84-121 (2017).
33. M. Huber, A. Goldner, Eocene monsoons. *Journal of Asian Earth Sciences* **44**, 3-23 (2012).
34. J. H. C. Bosmans, S. S. Drijfhout, E. Tuenter, F. J. Hilgen, L. J. Lourens, Response of the North African summer monsoon to precession and obliquity forcings in the EC-Earth GCM. *Climate Dynamics* **44**, 279-297 (2015).
35. H. Pälike *et al.*, The Heartbeat of the Oligocene Climate System. *Science* **314**, 1894-1898 (2006).
36. A. E. Holbourn, W. Kuhnt, S. Clemens, W. Prell, N. Andersen, Middle to late Miocene stepwise climate cooling: Evidence from a high-resolution deep water isotope curve spanning 8 million years. *Paleoceanography* **28**, 2013PA002538 (2013).
37. S. R. Meyers, L. A. Hinnov, Northern Hemisphere glaciation and the evolution of Plio-Pleistocene climate noise. *Paleoceanography* **25**, PA3207 (2010).

38. D. Liebrand, A. T. M. de Bakker, Bispectra of climate cycles show how ice ages are fuelled. *Clim. Past* **15**, 1959-1983 (2019).
39. S. Kirtland Turner, P. F. Sexton, C. D. Charles, R. D. Norris, Persistence of carbon release events through the peak of early Eocene global warmth. *Nature Geoscience* **7**, (2014).
40. D. J. Lunt et al., A model for orbital pacing of methane hydrate destabilization during the Palaeogene. *Nature Geosci* **4**, 775-778 (2011).
41. V. Dakos *et al.*, Slowing down as an early warning signal for abrupt climate change. *Proceedings of the National Academy of Sciences* **105**, 14308-14312 (2008).
42. M. Scheffer *et al.*, Early-warning signals for critical transitions. *Nature* **461**, 53-59 (2009).
43. W. Steffen *et al.*, Trajectories of the Earth System in the Anthropocene. *Proceedings of the National Academy of Sciences*, (2018).
44. M. D. Palmer, G. R. Harris, J. M. Gregory, Extending CMIP5 projections of global mean temperature change and sea level rise due to thermal expansion using a physically-based emulator. *Environmental Research Letters* **13**, 084003 (2018).

Supplementary References

45. J. C. Zachos, D. Kroon, P. Blum, et al., *Proc. ODP, Init. Repts., 208: College Station, TX (Ocean Drilling Program)*. (2004).
46. T. B. Coplen, Editorial: More uncertainty than necessary. *Paleoceanography* **11**, 369-370 (1996).
47. T. Westerhold, U. Röhl, T. Frederichs, S. M. Bohaty, J. C. Zachos, Astronomical calibration of the geological timescale: closing the middle Eocene gap. *Clim. Past* **11**, 1181-1195 (2015).
48. T. Westerhold et al., Late Lutetian Thermal Maximum—Crossing a Thermal Threshold in Earth's Climate System? *Geochemistry, Geophysics, Geosystems* **19**, 73-82 (2018).
49. S. J. Langton, N. M. Rabideaux, C. Borrelli, M. E. Katz, Southeastern Atlantic deep-water evolution during the late-middle Eocene to earliest Oligocene (Ocean Drilling Program Site 1263 and Deep Sea Drilling Project Site 366). *Geosphere* **12**, 1032-1047 (2016).
50. C. R. Riesselmann, R. B. Dunbar, D. A. Mucciarone, S. S. Kitasei, "High resolution stable isotope and carbonate variability during the early Oligocene climate transition: Walvis Ridge (ODP Site 1263)," *Open-File Report* (Reston, VA, 2007).
51. D. B. Bell, S. J. A. Jung, D. Kroon, L. J. Lourens, D. A. Hodell, Local and regional trends in Plio-Pleistocene d18O records from benthic foraminifera. **15**, 3304-3321 (2014).
52. T. Westerhold *et al.*, Astronomical calibration of the Ypresian timescale: implications for seafloor spreading rates and the chaotic behavior of the solar system? *Clim. Past* **13**, 1129-1152 (2017).
53. W. F. Ruddiman, D. Cameron, B. M. Clement, in *Init. Repts. DSDP, 94: Washington (U.S. Govt. Printing Office),* W. F. Ruddiman, R. B. Kidd, E. Thomas, et al., Eds. (1987), pp. 615-634.
54. R. Wilkens *et al.*, Revisiting the Ceara Rise, equatorial Atlantic Ocean: isotope stratigraphy of ODP Leg 154 from 0 to 5 Ma. *Clim Past* **13**, 799-793 (2017).

55. J. L. Kirschvink, The least-squares line and plane and the analysis of paleomagnetic data. *Geophys. J. Roy. Astron. Soc.* **62**, 699-718 (1980).
56. A. Stephenson, Gyromagnetism and the remanence acquired by a rotating rock in an alternating field. *Nature* **284**, 48-49 (1980).
57. A. Stephenson, Gyroremanent magnetization in a weakly anisotropic rock sample. *Physics of the Earth and Planetary Interiors* **25**, 163-166 (1981).
58. J. D. A. Zijderveld, in *Methods in Paleomagnetism,* D. W. Collinson, K. M. Creer, S. K. Runcorn, Eds. (Elsevier, Amsterdam, 1967), pp. 254-286.
59. P. C. Lurcock, F. Florindo, New developments in the PuffinPlot paleomagnetic data analysis program. *Geochemistry, Geophysics, Geosystems* **20**, (2019).
60. J. G. Ogg, in *The Geologic Time Scale,* F. M. Gradstein, J. G. Ogg, M. D. Schmitz, G. M. Ogg, Eds. (Elsevier, Boston, 2012), pp. 85-113.
61. F. J. Hilgen *et al.*, in *The Geologic Time Scale,* F. M. Gradstein, J. G. Ogg, M. D. Schmitz, G. M. Ogg, Eds. (Elsevier, Boston, 2012), pp. 923-978.
62. N. Vandenberghe *et al.*, in *The Geologic Time Scale,* F. M. Gradstein, J. G. Ogg, M. D. Schmitz, G. M. Ogg, Eds. (Elsevier, Boston, 2012), pp. 855-921.
63. S. Galeotti *et al.*, Cyclochronology of the Early Eocene carbon isotope record from a composite Contessa Road-Bottaccione section (Gubbio, central Italy). *Lethaia* **50**, 231-244 (2017).
64. S. C. Cande, D. V. Kent, A New Geomagnetic Polarity Time Scale for the late Cretaceous and Cenozoic. *Journal of Geophysical Research* **97**, 13,917-913,951 (1992).
65. S. C. Cande, D. V. Kent, Revised calibration of the geomagnetic polarity timescale for the Late Cretaceous and Cenozoic. *Journal of Geophysical Research* **100**, 6093-6095 (1995).
66. L. A. Hinnov, F. J. Hilgen, in *The Geologic Time Scale,* F. M. Gradstein, J. G. Ogg, M. D. Schmitz, G. M. Ogg, Eds. (Elsevier, Boston, 2012), pp. 63-83.
67. A. E. Holbourn et al., Late Miocene climate cooling and intensification of southeast Asian winter monsoon. *Nature Communications* **9**, 1584 (2018).
68. A. E. Holbourn et al., Middle Miocene climate cooling linked to intensification of eastern equatorial Pacific upwelling. *Geology* **42**, 19-22 (2014).
69. J. Laskar *et al.*, A long-term numerical solution for the insolation quantities of the Earth. *Astronomy and Astrophysics* **428**, 261-285 (2004).
70. K. Littler *et al.*, Astronomical Time Keeping of Earth History: An Invaluable Contribution of Scientific Ocean Drilling. *Oceanography* **32**, 72-76 (2019).
71. I. J. Kocken, M. J. Cramwinckel, R. E. Zeebe, J. J. Middelburg, A. Sluijs, The 405 kyr and 2.4 Myr eccentricity components in Cenozoic carbon isotope records. *Clim. Past* **15**, 91-104 (2019).
72. J. Laskar, in *Phil. Trans. R. Soc. Lond. A,* N. J. Shackleton, I. N. McCave, G. P. Weedon, Eds. (1999), vol. 357, pp. 1735-1759.
73. L. J. Lourens, F. J. Hilgen, J. Laskar, N. J. Shackleton, D. Wilson, in *A Geological Timescale 2004,* F. Gradstein, J. Ogg, A. Smith, Eds. (Cambridge University Press, Cambridge University Press, UK, 2004), pp. 409-440.
74. C. Zeeden, F. J. Hilgen, S. K. Hüsing, L. L. Lourens, The Miocene astronomical time scale 9–12 Ma: New constraints on tidal dissipation and their implications for paleoclimatic investigations. *Paleoceanography* **29**, 2014PA002615 (2014).

75. R. E. Zeebe, L. J. Lourens, Solar System chaos and the Paleocene–Eocene boundary age constrained by geology and astronomy. *Science* **365**, 926-929 (2019).
76. T. Westerhold, U. Röhl, J. Laskar, Time scale controversy: Accurate orbital calibration of the early Paleogene. *Geochem. Geophys. Geosyst.* **13**, Q06015 (2012).
77. J. S. K. Barnet *et al.*, A new high-resolution chronology for the late Maastrichtian warming event: Establishing robust temporal links with the onset of Deccan volcanism. *Geology* **46**, 147-150 (2017).
78. B. S. Cramer, J. D. Wright, D. V. Kent, M.-P. Aubry, Orbital climate forcing of d13C excursions in the late Paleocene - Eocene (chrons C24n-C25n). *Paleoceanography* **18**, 1097 (2003).
79. J. C. Zachos, H. McCarren, B. Murphy, U. Röhl, T. Westerhold, Tempo and scale of late Paleocene and early Eocene carbon isotope cycles: Implications for the origin of hyperthermals. *Earth and Planetary Science Letters* **299**, 242-249 (2010).
80. J. Laurin, B. Růžek, M. Giorgioni, Orbital Signals in Carbon Isotopes: Phase Distortion as a Signature of the Carbon Cycle. *Paleoceanography* **32**, 1236-1255 (2017).
81. N. J. Shackleton, M. A. Hall, A. Boersma, in *Initial Reports Deep Sea Drilling Project, vol. 74. US Governmental Printing Office, Washington,* T. C. Moore, P. D. Rabinowitz, Eds. (1984), pp. 599–613.
82. C. H. Lear, H. Elderfield, P. A. Wilson, Cenozoic Deep-Sea Temperatures and Global Ice Volumes from Mg/Ca in Benthic Foraminiferal Calcite. *Science* **287**, 269-272 (2000).
83. G. W. Brass, J. R. Southam, W. H. Peterson, Warm saline bottom water in the ancient ocean. *Nature* **296**, 620-623 (1982).
84. M. Huber, L. C. Sloan, Heat transport, deep waters, and thermal gradients: Coupled simulation of an Eocene greenhouse climate. *Geophysical Research Letters* **28**, 3481-3484 (2001).
85. K. L. Bice, J. Marotzke, Numerical evidence against reversed thermohaline circulation in the warm Paleocene/Eocene ocean. *Journal of Geophysical Research* **106**, 11,529-511,542 (2001).
86. M. Huber, R. Caballero, The early Eocene equable climate problem revisited. *Clim. Past* **7**, 603-633 (2011).
87. P. N. Pearson et al., Stable warm tropical climate through the Eocene Epoch. *Geology* **35**, 211-214 (2007).
88. J. S. K. Barnet et al., A High-Fidelity Benthic Stable Isotope Record of Late Cretaceous–Early Eocene Climate Change and Carbon-Cycling. *Paleoceanography and Paleoclimatology* **34**, 672-691 (2019).
89. J. P. Eckmann, S. O. Kamphorst, D. Ruelle, Recurrence Plots of Dynamical Systems. *Europhysics Letters (EPL)* **4**, 973-977 (1987).
90. K. H. Krämer, R. Donner, J. Heitzig, N. Marwan, Recurrence threshold selection for obtaining robust recurrence characteristics in different embedding dimensions. *Chaos* **28**, (2018).
91. N. Marwan, S. Schinkel, J. Kurths, Recurrence plots 25 years later - Gaining confidence in dynamical transitions. *EPL (Europhysics Letters)* **101**, 20007 (2013).
92. J. Hansen, M. Sato, G. Russell, P. Kharecha, Climate sensitivity, sea level and atmospheric carbon dioxide. *Philosophical Transactions of the Royal Society A: Mathematical, Physical and Engineering Sciences* **371**, 20120294 (2013).

93. J. Oerlemans, Correcting the Cenozoic $\delta^{18}O$ deep-sea temperature record for Antarctic ice volume. *Palaeogeography, Palaeoclimatology, Palaeoecology* **208**, 195-205 (2004).
94. G. L. Foster, D. L. Royer, D. J. Lunt, Future climate forcing potentially without precedent in the last 420 million years. *Nature Communications* **8**, 14845 (2017).
95. S. Ji *et al.*, A symmetrical CO2 peak and asymmetrical climate change during the middle Miocene. *Earth and Planetary Science Letters* **499**, 134-144 (2018).
96. T. B. Chalk *et al.*, Causes of ice age intensification across the Mid-Pleistocene Transition. *Proceedings of the National Academy of Sciences* **114**, 13114-13119 (2017).
97. R. Greenop *et al.*, Orbital Forcing, Ice Volume, and CO2 Across the Oligocene-Miocene Transition. *Paleoceanography and Paleoclimatology* **34**, 316-328 (2019).
98. L. Londoño *et al.*, Early Miocene CO_2 estimates from a Neotropical fossil leaf assemblage exceed 400 ppm. *American Journal of Botany* **105**, 1929-1937 (2018).
99. S. M. Sosdian *et al.*, Constraining the evolution of Neogene ocean carbonate chemistry using the boron isotope pH proxy. *Earth and Planetary Science Letters* **498**, 362-376 (2018).
100. M. Steinthorsdottir, V. Vajda, M. Pole, G. Holdgate, Moderate levels of Eocene pCO_2 indicated by Southern Hemisphere fossil plant stomata. *Geology*, (2019).
101. J. R. Super *et al.*, North Atlantic temperature and pCO_2 coupling in the early-middle Miocene. *Geology* **46**, 519-522 (2018).
102. G. E. A. Swann, C. P. Kendrick, A. J. Dickson, S. Worne, Late Pliocene Marine pCO_2 Reconstructions From the Subarctic Pacific Ocean. *Paleoceanography and Paleoclimatology* **33**, 457-469 (2018).
103. C. R. Witkowski, J. W. H. Weijers, B. Blais, S. Schouten, J. S. Sinninghe Damsté, Molecular fossils from phytoplankton reveal secular pCO_2 trend over the Phanerozoic. *Science Advances* **4**, eaat4556 (2018).
104. A. P. Wolfe *et al.*, Middle Eocene CO_2 and climate reconstructed from the sediment fill of a subarctic kimberlite maar. *Geology* **45**, 619-622 (2017).
105. J. C. G. Walker, P. B. Hays, J. K. Kasting, A negative feedback mechanism for the long term stabilization of Earth´s surface temperature. *Journal of Geophysical Research* **86**, 9776-9782 (1981).
106. R. A. Berner, A model of atmospheric CO_2 over Phanerozoic time. *American Journal of Science* **291**, 339-376 (1991).
107. A. Holbourn, W. Kuhnt, M. Schulz, H. Erlenkeuser, Impacts of orbital forcing and atmospheric carbon dioxide on Miocene ice-sheet expansion. *Nature* **438**, 483-487 (2005).
108. S. C. Woodard et al., Antarctic role in Northern Hemisphere glaciation. *Science* **346**, 847-851 (2014).
109. M. R. Saltzman, E. Thomas, in *The Geologic Time Scale,* F. M. Gradstein, J. G. Ogg, M. D. Schmitz, G. M. Ogg, Eds. (Elsevier, Boston, 2012), pp. 207-232.
110. J. C. Zachos, M. A. Arthur, W. E. Dean, Geochemical Evidence for Suppression of Pelagic Marine Productivity at the Cretaceous/Tertiary Boundary. *Nature* **337**, 61-64 (1989).
111. A. K. Hilting, L. R. Kump, T. J. Bralower, Variations in the oceanic vertical carbon isotope gradient and their implications for the Paleocene-Eocene biological pump. *Paleoceanography* **23**, (2008).

112. A. C. Kurtz, L. R. Kump, M. A. Arthur, J. C. Zachos, A. Paytan, Early Cenozoic decoupling of the global carbon and sulfur cycles. *Paleoceanography* **18**, 1090, (2003).
113. E. Vincent, W. H. Berger, in *The carbon cycle and atmospheric CO_2: Natural variations Archean to Present.,* E. T. Sundquist, W. S. Broecker, Eds. (AGU, Washington D. C., 1985), pp. 455-468.
114. A. J. Drury, C. e. d. M. John, A. E. Shevenell, Evaluating climatic response to external radiative forcing during the late Miocene to early Pliocene: New perspectives from eastern equatorial Pacific (IODP U1338) and North Atlantic (ODP 982) locations. *Paleoceanography* **31**, 167-184 (2016).
115. L. J. Lourens *et al.*, Astronomical pacing of late Palaeocene to early Eocene global warming events. *Nature* **435**, 1083-1087 (2005).
116. B. S. Slotnick *et al.*, Large-Amplitude Variations in Carbon Cycling and Terrestrial Weathering during the Latest Paleocene and Earliest Eocene: The Record at Mead Stream, New Zealand. *The Journal of Geology* **120**, 487-505 (2012).
117. G. R. Dickens, Rethinking the global carbon cycle with a large, dynamic and microbially mediated gas hydrate capacitor. *Earth and Planetary Science Letters* **213**, 169-183 (2003).
118. D. L. Royer, CO_2-forced climate thresholds during the Phanerozoic. *Geochimica et Cosmochimica Acta* **70**, 5665-5675 (2006).
119. J. D. Hays, J. Imbrie, N. J. Shackleton, Variations in the Earth's Orbit: pacemaker of the Ice Ages. *Science* **194**, 1121-1132 (1976).
120. D. Liebrand et al., Cyclostratigraphy and eccentricity tuning of the early Oligocene through early Miocene (30.1–17.1 Ma): Cibicides mundulus stable oxygen and carbon isotope records from Walvis Ridge Site 1264. *Earth and Planetary Science Letters* **450**, 392-405 (2016).
121. H. M. Beddow, D. Liebrand, A. Sluijs, B. S. Wade, L. J. Lourens, Global change across the Oligocene-Miocene transition: High-resolution stable isotope records from IODP Site U1334 (equatorial Pacific Ocean). *Paleoceanography* **31**, 81-97 (2016).
122. D. J. Thomson, Spectrum estimation and harmonic analysis. *Proceedings of the IEEE* **70**, 1055-1096 (1982).
123. K. Billups, H. Palike, J. E. T. Channell, J. C. Zachos, N. J. Shackleton, Astronomic calibration of the late Oligocene through early Miocene geomagnetic polarity time scale. *Earth and Planetary Science Letters* **224**, 33-44 (2004).
124. N. J. Shackleton, S. J. Crowhurst, G. P. Weedon, J. Laskar, in *Phil. Trans. R. Soc. Lond. A*, N. J. Shackleton, I. N. McCave, G. P. Weedon, Eds. (1999), vol. **357**, pp. 1907-1929.
125. G. P. Weedon, N. J. Shackleton, P. N. Pearson, in *Proc. ODP, Sci. Results*, **154**: College Station, TX (Ocean Drilling Program), N. J. Shackleton, W. B. Curry, C. Richter, T. J. Bralower, Eds. (1997), pp. 101-114.
126. H. Pälike, J. Frazier, J. C. Zachos, Extended orbitally forced palaeoclimatic records from the equatorial Atlantic Ceara Rise. *Quaternary Science Reviews* **25**, 3138-3149 (2006).
127. J. Zachos, N. J. Shackleton, J. S. Revenaugh, H. Pälike, B. P. Flower, Climate Response to Orbital Forcing Across the Oligocene-Miocene Boundary. *Science* **292**, 274-278 (2001).
128. J. C. Zachos, B. P. Flower, H. Paul, Orbitally paced climate oscillations across the Oligocene/Miocene boundary. *Nature* **388**, 567-570 (1997).

129. IPCC, *Climate Change 2013: The Physical Science Basis. Contribution of Working Group I to the Fifth Assessment Report of the Intergovernmental Panel on Climate Change*. T. F. Stocker *et al.*, Eds., (Cambridge University Press, Cambridge United Kingdom and New York, NY, USA, 2013).
130. C. J. Hollis *et al.*, The DeepMIP contribution to PMIP4: methodologies for selection, compilation and analysis of latest Paleocene and early Eocene climate proxy data, incorporating version 0.1 of the DeepMIP database. *Geosci. Model Dev.* **12**, 3149-3206 (2019).
131. E. Anagnostou et al., Changing atmospheric CO_2 concentration was the primary driver of early Cenozoic climate. *Nature* **533**, 380-384 (2016).
132. P. N. Pearson, M. R. Palmer, Atmospheric carbon dioxide concentrations over the past 60 million years. *Nature* **406**, 695-699 (2000).
133. Y. G. Zhang, M. Pagani, Z. Liu, S. M. Bohaty, R. Deconto, A 40-million-year history of atmospheric CO_2. *Philos Trans A Math Phys Eng Sci* **371**, 20130096 (2013).
134. K. D. Burke *et al.*, Pliocene and Eocene provide best analogs for near-future climates. *Proceedings of the National Academy of Sciences*, 201809600 (2018).
135. E. Gasson, R. M. DeConto, D. Pollard, R. H. Levy, Dynamic Antarctic ice sheet during the early to mid-Miocene. *Proceedings of the National Academy of Sciences* **113**, 3459-3464 (2016).
136. M. A. Kominz *et al.*, Late Cretaceous to Miocene sea-level estimates from the New Jersey and Delaware coastal plain coreholes: an error analysis. *Basin Research* **20**, 211-226 (2008).
137. K. G. Miller, J. D. Wright, J. V. Browning, Visions of ice sheets in a greenhouse world. *Marine Geology* **217**, 215-231 (2005).
138. A. E. Shevenell, J. P. Kennett, D. W. Lea, Middle Miocene ice sheet dynamics, deep-sea temperatures, and carbon cycling: A Southern Ocean perspective. *Geochemistry, Geophysics, Geosystems* **9**, (2008).
139. M. Meinshausen *et al.*, The RCP greenhouse gas concentrations and their extensions from 1765 to 2300. *Climatic Change* **109**, 213-241 (2011).
140. R. M. DeConto, D. Pollard, Rapid Cenozoic glaciation of Antarctica induced by declining atmospheric CO2. *Nature* **421**, 245-249 (2003).
141. G. Doria *et al.*, Declining atmospheric CO_2 during the late Middle Eocene climate transition. *American Journal of Science* **311**, 63-75 (2011).
142. P. N. Pearson, Oxygen Isotopes in Foraminifera: Overview and Historical Review. *The Paleontological Society Papers* **18**, 1-38 (2012).
143. J. Bloch-Johnson, R. T. Pierrehumbert, D. S. Abbot, Feedback temperature dependence determines the risk of high warming. *Geophysical Research Letters* **42**, 4973-4980 (2015).
144. R. Caballero, M. Huber, State-dependent climate sensitivity in past warm climates and its implications for future climate projections. *Proceedings of the National Academy of Sciences* **110**, 14162-14167 (2013).
145. C. F. Dawber, A. K. Tripati, Exploring the controls on element ratios in middle Eocene samples of the benthic foraminifera Oridorsalis umbonatus. *Clim. Past* **8**, 1957-1971 (2012).

146. C. F. Dawber, A. K. Tripati, A. S. Gale, C. MacNiocaill, S. P. Hesselbo, Glacioeustasy during the middle Eocene? Insights from the stratigraphy of the Hampshire Basin, UK. *Palaeogeography, Palaeoclimatology, Palaeoecology* **300**, 84-100 (2011).
147. A. Dutton, K. C. Lohmann, R. M. Leckie, Insights from the Paleocene tropical Pacific: Foraminiferal stable isotope and elemental results from Site 1209, Shatsky Rise. *Paleoceanography* **20**, (2005).
148. S. R. Meyers. (2014). Astrochron: An R Package for Astrochronology, available at: https://CRAN.R-project.org/package=astrochron
149. C. Torrence, G. P. Compo, A Practical Guide to Wavelet Analysis. *Bulletin of the American Meteorological Society* **79**, 61-78 (1998).
150. A. Grinsted, J. C. Moore, S. Jevrejeva, Application of the cross wavelet transform and wavelet coherence to geophysical time series. *Nonlin. Processes Geophys*. **11**, 561-566 (2004).
151. D. Paillard, L. Labeyrie, P. Yiou, Macintosh Program performs time-series analysis. *Eos, Transactions American Geophysical Union* **77**, 379-379 (1996).
152. M. Meinshausen *et al.*, Historical greenhouse gas concentrations for climate modelling (CMIP6). *Geosci. Model Dev.* **10**, 2057-2116 (2017).
153. C. P. Morice, J. J. Kennedy, N. A. Rayner, P. D. Jones, Quantifying uncertainties in global and regional temperature change using an ensemble of observational estimates: The HadCRUT4 data set. *Journal of Geophysical Research: Atmospheres* **117**, (2012).
154. C. N. Waters *et al.*, The Anthropocene is functionally and stratigraphically distinct from the Holocene. *Science* **351**, aad2622 (2016).
155. C. Zeeden *et al.*, Revised Miocene splice, astronomical tuning and calcareous plankton biochronology of ODP Site 926 between 5 and 14.4 Ma. *Palaeogeography, Palaeoclimatology, Palaeoecology* **369**, 430-451 (2013).
156. T. Westerhold *et al.*, Orbitally tuned timescale and astronomical forcing in the middle Eocene to early Oligocene. *Clim. Past* **10**, 955-973 (2014).
157. L. Rivero-Cuesta et al., Paleoenvironmental Changes at ODP Site 702 (South Atlantic): Anatomy of the Middle Eocene Climatic Optimum. *Paleoceanography and Paleoclimatology* **n/a**, (2019).
158. N. J. Shackleton, M. A. Hall, D. Pate, in Supplement to: Shackleton, NJ et al. (1995): Pliocene stable isotope stratigraphy of Site 864. In: Pisias, NG; Mayer, LA; Janecek, TR; Palmer-Julson, A; van Andel, TH (eds.), *Proceedings of the Ocean Drilling Program*, Scientific Results, College Station, TX (Ocean Drilling Program), **138**, 337-355, (1995).
159. T. Bickert, W. B. Curry, G. Wefer, in *Proc. ODP, Sci. Results, 154: College Station, TX (Ocean Drilling Program),* N. J. Shackelton, W. B. Curry, C. Richter, T. J. Bralower, Eds. (1997), pp. 239-254.
160. N. J. Shackleton, M. A. Hall, in Proc. ODP, Sci. Results, 154: College Station, TX (Ocean Drilling Program), N. J. Shackleton, W. B. Curry, C. Richter, T. J. Bralower, Eds. (1997), vol. **154**, pp. 367-373.
161. N. J. Shackleton, N. D. Opdyke, Oxygen isotope and palaeomagnetic stratigraphy of Equatorial Pacific core V28-238: Oxygen isotope temperatures and ice volumes on a 10^5 year and 10^6 year scale. *Quaternary Research* **3**, 39-55 (1973).
162. P. F. Sexton *et al.*, Eocene global warming events driven by ventilation of oceanic dissolved organic carbon. *Nature* **471**, 349-352 (2011).

163. K. Billups, A. C. Ravelo, J. C. Zachos, Early Pliocene deep water circulation in the western equatorial Atlantic: Implications for high-latitude climate change. *Paleoceanography* **13**, 84-95 (1998).
164. P. deMenocal, D. Archer, P. Leth, in *Proc. ODP, Sci. Results, 154: College Station, TX (Ocean Drilling Program),* N. J. Shackelton, W. B. Curry, C. Richter, T. J. Bralower, Eds. (1997), pp. 285-298.
165. S. O. Franz, R. Tiedemann. Stable isotope data of Hole 154-925C (Tab. A2) (PANGAEA, 2002). 10.1594/PANGAEA.67526.
166. J. Tian et al., Paleoceanography of the east equatorial Pacific over the past 16 Myr and Pacific–Atlantic comparison: High resolution benthic foraminiferal $\delta^{18}O$ and $\delta^{13}C$ records at IODP Site U1337. *Earth and Planetary Science Letters* **499**, 185-196 (2018).
167. R. Tiedemann, S. O. Franz, in *Proc. ODP, Sci. Results, 154: College Station, TX (Ocean Drilling Program),* N. J. Shackelton, W. B. Curry, C. Richter, T. J. Bralower, Eds. (1997), pp. 299-318.
168. F. Boscolo Galazzo *et al.*, The middle Eocene climatic optimum (MECO): A multiproxy record of paleoceanographic changes in the southeast Atlantic (ODP Site 1263, Walvis Ridge). *Paleoceanography* **29**, 2014PA002670 (2014).
169. H. K. Coxall, P. A. Wilson, Early Oligocene glaciation and productivity in the eastern equatorial Pacific: Insights into global carbon cycling. *Paleoceanography* **26**, PA2221 (2011).
170. A. Holbourn, W. Kuhnt, M. Schulz, J.-A. Flores, N. Andersen, Orbitally-paced climate evolution during the middle Miocene "Monterey" carbon-isotope excursion. *Earth and Planetary Science Letters* **261**, 534-550 (2007).
171. C. H. Lear, Y. Rosenthal, H. K. Coxall, W. P. A., Late Eocene to early Miocene ice sheet dynamics and the global carbon cycle. *Paleoceanography* **19**, (2004).
172. D. Liebrand et al., Antarctic ice sheet and oceanographic response to eccentricity forcing during the early Miocene. Clim. Past 7, 869-880 (2011).
173. J. Tian, W. Ma, M. W. Lyle, J. K. Shackford, Synchronous mid-Miocene upper and deep oceanic $\delta^{13}C$ changes in the east equatorial Pacific linked to ocean cooling and ice sheet expansion. *Earth and Planetary Science Letters* **406**, 72-80 (2014).
174. V. Lauretano, F. J. Hilgen, J. C. Zachos, L. J. Lourens, Astronomically tuned age model for the early Eocene carbon isotope events: A new high-resolution $\delta^{13}C$ benthic record of ODP Site 1263 between ~49 and ~54 Ma. *Newsletters on Stratigraphy* **49**, 383–400 (2016).
175. V. Lauretano, K. Littler, M. Polling, J. C. Zachos, L. J. Lourens, Frequency, magnitude and character of hyperthermal events at the onset of the Early Eocene Climatic Optimum. *Clim. Past* **11**, 1313-1324 (2015).
176. B. S. Wade, H. Pälike, Oligocene climate dynamics. *Paleoceanography* **19**, PA4019 (2004).
177. K. Littler, U. Röhl, T. Westerhold, J. C. Zachos, A high-resolution benthic stable-isotope record for the South Atlantic: Implications for orbital-scale changes in Late Paleocene–Early Eocene climate and carbon cycling. *Earth and Planetary Science Letters* **401**, 18-30 (2014).
178. L. Stap *et al.*, High-resolution deep-sea carbon and oxygen isotope records of Eocene Thermal Maximum 2 and H2. *Geology* **38**, 607-610 (2010).

179. E. Thomas *et al.*, Early Eocene Thermal Maximum 3: Biotic Response at Walvis Ridge (SE Atlantic Ocean). *Paleoceanography and Paleoclimatology* **33**, 862–883 (2018).
180. P. M. Hull et al., On impact and volcanism across the Cretaceous-Paleogene boundary. *Science* **367**, 266-272 (2020).
181. V. Lauretano, J. C. Zachos, L. J. Lourens, Orbitally Paced Carbon and Deep-Sea Temperature Changes at the Peak of the Early Eocene Climatic Optimum. *Paleoceanography and Paleoclimatology* **33**, 1050-1065 (2018).

Acknowledgments: We thank Henning Kuhnert and his team for stable isotope analyses at MARUM, and the teams at the IODP Gulf Coast Core Repository (GCR) and the IODP Bremen Core Repository (BCR) for sampling. **Funding:** This research used samples and/or data provided by the International Ocean Discovery Program (IODP). Funding for this research was provided by the Deutsche Forschungsgemeinschaft (DFG, German Research Foundation) to TW (Project numbers 320221997, 242225091), UR (Project numbers 5410858, 28504316, 179386126, 242241969, 320221997); AH (Project numbers 48739182, 224193684 and 142157224); the Natural Environmental Research Council (NERC) to DAH; the DFG (Project numbers 386137731, 405856037) and the European Union's Horizon 2020 research and innovation program under grant agreement No 820970 to NM; the DFG (Project number 408101468) and by the European Union's Horizon 2020 research and innovation programme under the Marie Sklodowska-Curie grant agreement No 796220 to AJD; the National Science Foundation of China (Grant No. 41525020, 41776051) to JT; the NERC Isotope Geosciences Facility at the British Geological Survey (IP-1581–1115) to JB and KL; the NWO-ALW grant (project number 865.10.001) and Netherlands Earth System Science Centre (gravitation grant number 024.002.001) to LJL; the NSF (grant number EAR-0628719) to J.Z.. Funded through the Cluster of Excellence ›The Ocean Floor – Earth's Uncharted Interface‹ (research unit Recorder).
Author contributions: TW, UR, AJD, JCZ designed the study; TW, AJD, DL, DDV compiled and revised the astrochronology; NM applied recurrence analysis; EA synthesized the pCO_2 data; CA evaluated calcareous nannofossil datums; FF and TF produced magnetostratigraphic results and interpretation for ODP 1263; DAH, AJD, TW, UR provided bulk and benthic isotope data; AJD and RHW wrote the code for data processing and interpretation; JSKB, SMB, AJD, NM, AEH, DK, VL, KL, LJL, ML, HP, JT, PAW, UR, TW designed projects and generated data basis for the reference record as well as discussed/modified the manuscript. All authors contributed to writing the final manuscript. **Competing interests:** The authors declare no competing interests. **Data and materials availability:** All data are available in the main text or in the supplementary materials. All data are available open access in electronic form at the PANGAEA data repository (www. pangaea.de) http://doi.pangaea.de/ 10.1594/PANGAEA.10.1594/PANGAEA.917503.

Supplementary Materials:

Materials and Methods

Supplementary Text S1-S4

Figures S1-S35

Tables S1-S7

Data S8-S34

References (*45-181*)

Fig. 1. Cenozoic Global Reference benthic carbon and oxygen Isotope Dataset (CENOGRID) from ocean drilling core sites spanning the past 66 million years. Data are mostly generated using benthic foraminifera tests of the taxa *Cibicidoides* and *Nuttalides* extracted from carbonate rich deep-sea sediments drilled during ODP / IODP expeditions. Genus-specific corrections were applied and oxygen isotope data adjusted by +0.64‰ and +0.4‰, respectively (*12*), with the green dot indicating the average oxygen isotope composition of the last 10 kyr. Average resolution for the last 34 million years is one sample every 2 kyr, for the interval from 34 to 67 million years 4.4 kyr. After binning data were resampled and smoothed by a locally weighted function over 20 kyr (blue curve) and 1 Myr (red curve) to accentuate the different rhythms and trends in Earth's carbon cycle and temperature operating on various time scales. Oxygen isotope data have been converted to average temperature differences with respect to today (*13*). Future projections for global temperature (*44*) in the Year 2300 are shown by plotting three Representative Concentration Pathways (RCP) scenarios are plotted (light and dark blue, red dots). Gray horizontal bars mark rough estimates of ice volume in each hemisphere. Absolute ages for epochs and stages of the Cenozoic (GTS2012) and geomagnetic field reversals (this study) are provided for reference. Note that the oxygen isotope data axis is reversed to reflect warmer temperatures at times of lower $\delta^{18}O$ values. K/Pg is the Cretaceous/Paleogene boundary, Oi-1 is the first major glacial period in the Oligocene, M2 is the first major glacial event in the Northern Hemisphere.

Fig. 2. Climate states of the Cenozoic. Deep-sea benthic foraminifer high-resolution carbon (A) and oxygen (B) isotope records and the respective recurrence plots as well as scatter plots of long-term benthic foraminifer carbon versus oxygen values (C) and oxygen values versus atmospheric CO_2 concentrations (D). Recurrence analysis compares climate change patterns occurring in a specific interval to the entire record. If climate dynamics have similar patterns they will show up as darker areas in the plot, if they have no common dynamics the plot will remain white. Four distinct climate states can be identified as Hothouse, Warmhouse, Coolhouse, and Icehouse with distinct transitions among them. The relation of oxygen isotopes, representative for average global temperature trends, to atmospheric CO_2 concentrations suggests that the present climate system as of today (415 ppm CO_2) is comparable to the Miocene Coolhouse close to the Miocene Climate Optimum. If CO_2 emissions continue unmitigated until 2100 as assumed for the RCP8.5 scenario, the Earth climate system will be moved abruptly from the Icehouse into the Warmhouse or even Hothouse climate state.

Fig. 3. Quasi-periodic changes and determinism in the global reference carbon cycle and oxygen isotope record. Evolutionary FFT spectrogram, recurrence determinism analysis and benthic foraminifer oxygen (A) and carbon (B) isotope data plotted on age with the four climate states. Frequencies between two and sixty cycles per million years are related to changes in Earth's orbital parameters, known as Milankovitch cycles. The FFT spectrograms were computed with a 5-Myr window on the detrended records of benthic carbon and oxygen isotope data. From 67 to 13.9 Ma cyclic variations in global climate are dominated by the 405- and 100-kyr eccentricity cycles. Thereafter, in particular in the oxygen isotope record, the influence of obliquity increased, dominating the rhythm of climate in the record younger than ~7.7 million years. Recurrence analysis of determinism (DET) shows that climate in the Warmhouse state is more deterministic (predictable) than in the Hot-, Cool- and Icehouse. From 47 Ma towards the Eocene-Oligocene Transition at 34 Ma climate dynamic changes are rising in amplitude

approaching a threshold in the Climate System. If DET tends to low values, the dynamics are stochastic, whereas high values represent deterministic dynamics.

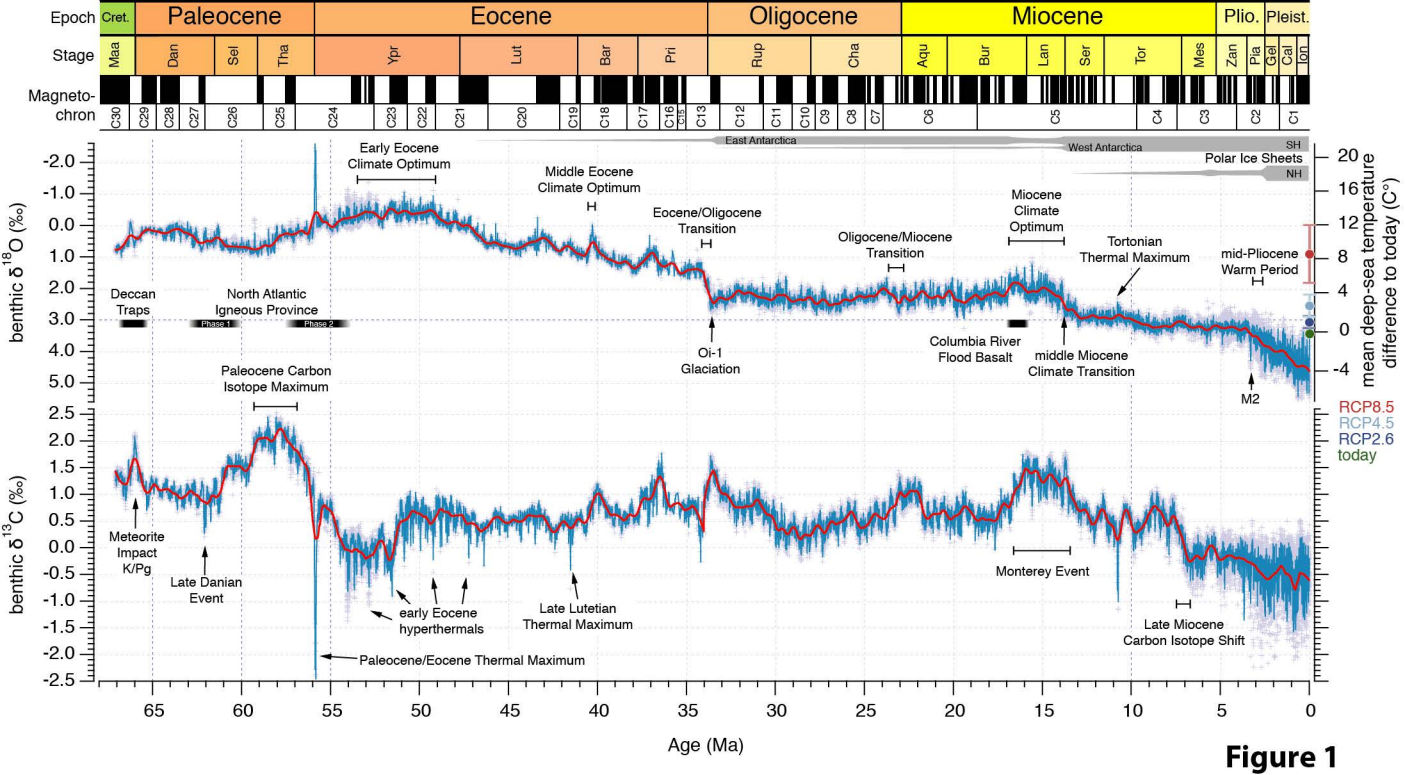
Epoch
Cret.
Paleocene
Eocene
Oligocene
Miocene
Plio.
Pleist.
Stage
Maa
Dan
Sel
Tha
Ypr
Lut
Bar
Pri
Rup
Cha
Aqu
Bur
Lan
Ser
Tor
Mes
Zan
Pia
Gel
Cal
Tgn
Magneto-chron
C30
C29
C28
C27
C26
C25
C24
C23
C22
C21
C20
C19
C18
C17
C16
C15
C13
C12
C11
C10
C9
C8
C7
C6
C5
C4
C3
C2
C1
East Antarctica
West Antarctica
SH
Polar Ice Sheets
NH
Early Eocene Climate Optimum
Middle Eocene Climate Optimum
Eocene/Oligocene Transition
Oligocene/Miocene Transition
Miocene Climate Optimum
Tortonian Thermal Maximum
mid-Pliocene Warm Period
Deccan Traps
North Atlantic Igneous Province
Phase 1
Phase 2
Paleocene Carbon Isotope Maximum
Oi-1 Glaciation
Columbia River Flood Basalt
middle Miocene Climate Transition
M2
benthic δ18O (‰)
mean deep-sea temperature difference to today (C°)
RCP8.5
RCP4.5
RCP2.6
today
benthic δ13C (‰)
Meteorite Impact K/Pg
Late Danian Event
early Eocene hyperthermals
Late Lutetian Thermal Maximum
Paleocene/Eocene Thermal Maximum
Monterey Event
Late Miocene Carbon Isotope Shift
Age (Ma)

Figure 1

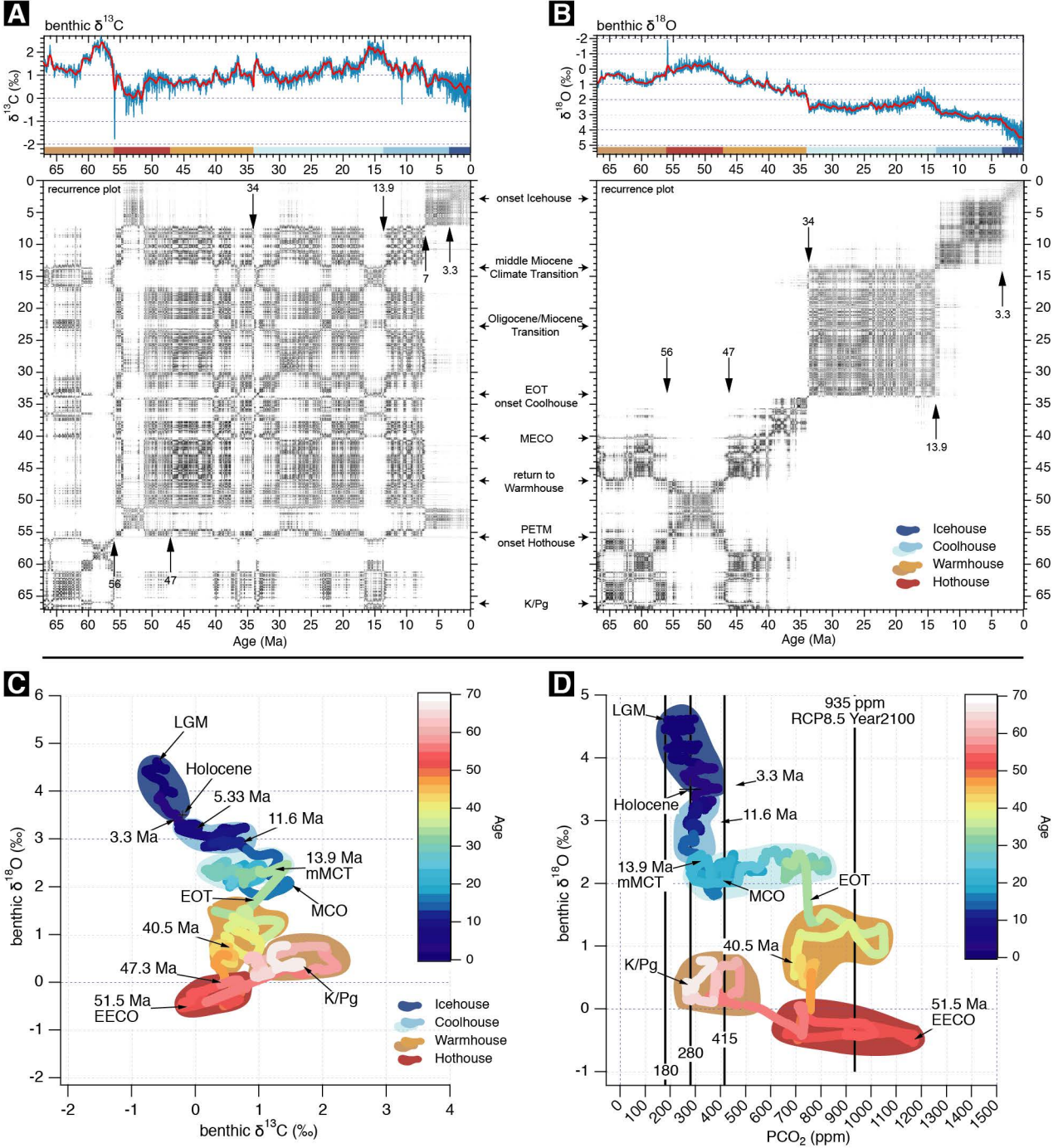
A
benthic δ13C
δ13C (‰)
recurrence plot
34
13.9
7
3.3
56
47
onset Icehouse
middle Miocene Climate Transition
Oligocene/Miocene Transition
EOT onset Coolhouse
MECO
return to Warmhouse
PETM onset Hothouse
K/Pg
Age (Ma)
B
benthic δ18O
δ18O (‰)
recurrence plot
34
3.3
56
47
13.9
Icehouse
Coolhouse
Warmhouse
Hothouse
Age (Ma)
C
LGM
Holocene
5.33 Ma
11.6 Ma
3.3 Ma
13.9 Ma
mMCT
EOT
MCO
40.5 Ma
47.3 Ma
51.5 Ma
EECO
K/Pg
Icehouse
Coolhouse
Warmhouse
Hothouse
benthic δ18O (‰)
benthic δ13C (‰)
Age
D
935 ppm
RCP8.5 Year2100
LGM
3.3 Ma
Holocene
11.6 Ma
13.9 Ma
mMCT
MCO
EOT
40.5 Ma
K/Pg
51.5 Ma
EECO
180
280
415
benthic δ18O (‰)
PCO2 (ppm)
Age

Figure 2

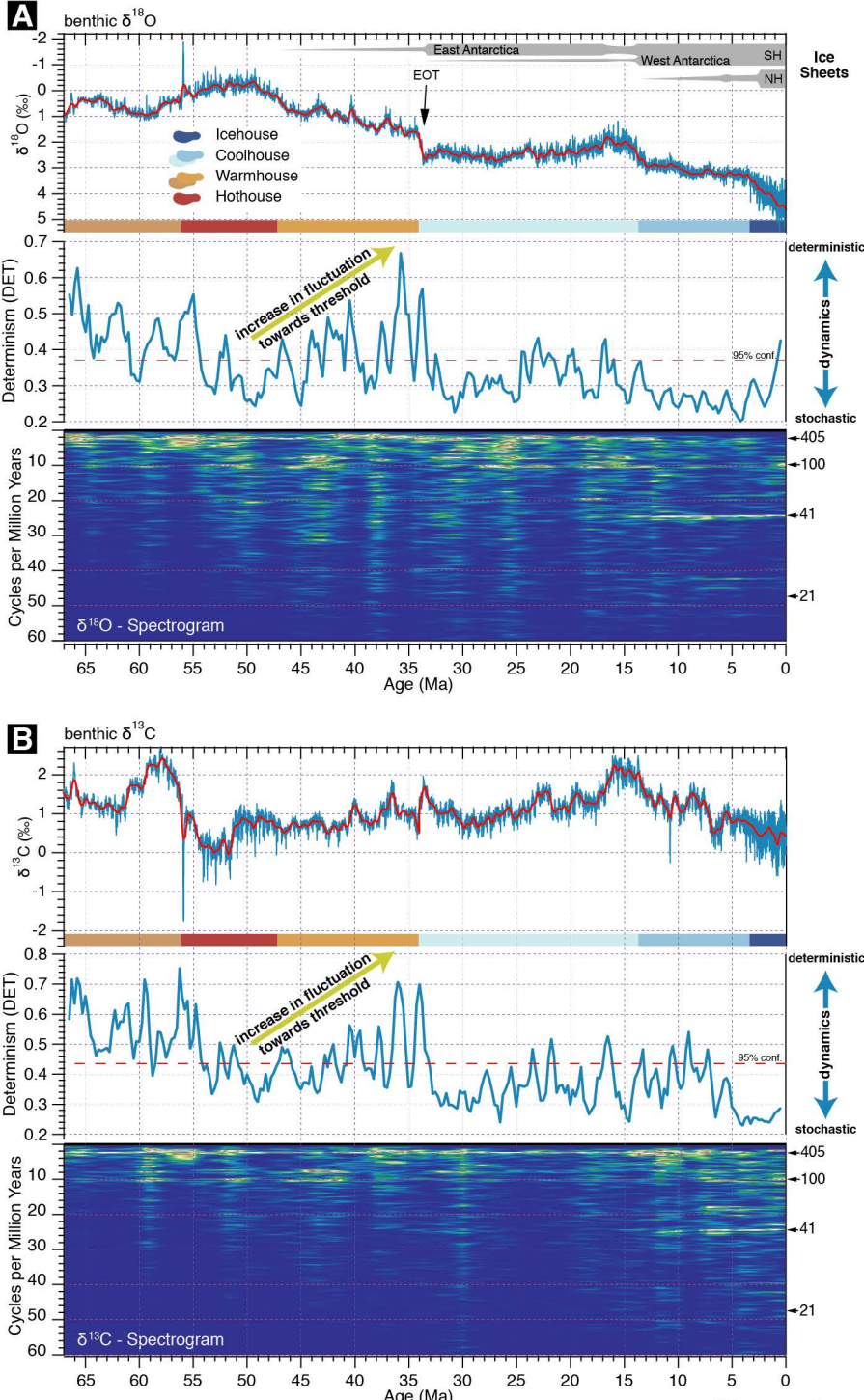
A
benthic δ18O
East Antarctica
West Antarctica
SH
NH
Ice Sheets
EOT
δ18O (‰)
Icehouse
Coolhouse
Warmhouse
Hothouse
Determinism (DET)
increase in fluctuation towards threshold
95% conf.
deterministic
dynamics
stochastic
Cycles per Million Years
405
100
41
21
δ18O - Spectrogram
Age (Ma)
B
benthic δ13C
δ13C (‰)
Determinism (DET)
increase in fluctuation towards threshold
95% conf.
deterministic
dynamics
stochastic
Cycles per Million Years
405
100
41
21
δ13C - Spectrogram
Age (Ma)

Figure 3